RSC Advances

PAPER

View Article Online
View Journal | View Issue

Cite this: *RSC Adv.*, 2024, **14**, 30055

MOF@platelet-rich plasma antimicrobial GelMA dressing: structural characterization, biocompatibility, and effect on wound healing efficacy

Pengyu Huang,†[ad] Yongan He,†*[b] Chunnuan Huang,†[a] Shuhan Jiang,[a] Ji Gan,[a] Rong Wu,[a] Chengjiao Ai,[a] Jiean Huang,*[a] Chaoguang Yao*[c] and Quanzhi Chen *[a]

In this study, a metal–organic framework (MOF) antimicrobial gel loaded with platelet-rich plasma (PRP) was prepared to improve the biological properties of gelatin gels and enhance their wound healing efficiency. PRP, MOF particles, and PRP-loaded MOF particles were each integrated into gelatin gels. The performance of the gels was evaluated for micro-structure, mechanical strength, *in vitro* biocompatibility and pro-wound healing effects. The results revealed that the integration of PRP created a multi-cross-linked structure, increasing the ductility of the gels by over 40%. The addition of MOF particles significantly increased the strength of the gel from 13 kPa to 43 kPa. The combination of MOF and PRP further improved the cell induction and migration capabilities of the composite gel, and the scratches in the PRP/MOF@GelMA group had completely healed within 48 h. Due to the presence of MOF and PRP, the gel dressing exhibited inhibitory effects of 45.7% against *Staphylococcus aureus* (*S. aureus*) and 50.2% against *Escherichia coli* (*E. coli*). Different gels promoted tissue regeneration and wound healing ability of bacterial-infected wounds in C57 rats, while PRP/MOF@GelMA showed the strongest wound repair ability with 100% healing. This study provides a new strategy for the development and clinical application of gel dressings.

Received 21st June 2024
Accepted 11th September 2024

DOI: 10.1039/d4ra04546g

rsc.li/rsc-advances

1. Introduction

In everyday life, it is often difficult to avoid damage to human skin from external stimuli, which in turn leads to a temporary or permanent loss of function (Sorg H., *et al.*, 2017; Qi L., *et al.*, 2022).[1,2] Wound healing is a complex and dynamic physiological process consisting of four key phases: hemostasis, inflammation, proliferation and remodeling (Cheng Y., *et al.*, 2019; Negut I., *et al.*, 2018).[3,4] During these stages, a series of tightly regulated events occur, such as phagocytosis, chemotaxis, collagen degradation, and remodeling (Kim H. S., *et al.*, 2019).[5] If bacterial infection occurs at the wound site, it will seriously hinder wound healing and may even be life-threatening (Gurtner G. C., *et al.*, 2008).[6] Common treatments for chronic wounds include tissue debridement, dressings, and antibiotics (Bowers S., *et al.*, 2020, Volmer-Thole M., *et al.*, 2016).[7,8] However, traditional dressings, such as gauze, have drawbacks including the shortage of antibacterial properties, poor water retention performance, easy adherence to the wound surface, inadequate adaptability to wound shapes, and an inability to provide growth factors, all of which limit their effectiveness in clinical practice. Additionally, there is concern that the overuse of antibiotics will lead to drug resistance (Davies J., *et al.*, 2010; Urban-Chmiel R., *et al.*, 2022).[9,10] Traditional methods do not fully address the needs of chronic wound healing, highlighting the urgent need to develop novel multifunctional dressings and antimicrobial agents that can provide more effective antimicrobial therapy and promote wound healing.

Hydrogels show great potential in wound repair applications, particularly GelMA, which is derived from gelatin and has been extensively studied as a dressing material (Yue K., *et al.*, 2015; Kurian A. G., *et al.*, 2012).[11,12] It possesses excellent biocompatibility and biodegradable properties, making it a popular choice for dressings that promote hemostasis and wound healing. The structure of GelMA contains the RGD (Arg-Gly-Asp) protein sequence, which effectively promotes cell adhesion, proliferation, differentiation, and tissue remodeling (Liu Y., *et al.*, 2022; Zhou Z., *et al.*, 2023; Jiang G., *et al.*, 2021).[13–15] Studies have shown that GelMA is compatible with various cell types, including human epidermal keratinocytes, epithelial fibroblasts, and bone marrow mesenchymal stem cells, without affecting their proliferation and metabolism

[a]*School of Basic Medical Sciences, The Second Affiliated Hospital, Guangxi Medical University, Nanning 530021, Guangxi, P. R. China. E-mail: quanzhi_chen@163.com; hjagxmu@163.com*

[b]*Department of Gastroenterology, The People's Hospital of Chongzuo, Chongzuo, 532200, Guangxi, P. R. China. E-mail: hyamail@qq.com*

[c]*Department of Gastroenterology, Hechi People's Hospital, Hechi, 547000, Guangxi, P. R. China. E-mail: ychg1975@163.com*

[d]*Department of Gastroenterology, People's Hospital of Guangxi Zhuang Autonomous Region, Nanning, 530021, Guangxi, P. R. China*

† These authors contributed equally to this work.

during co-culture (Nuutila K., *et al.*, 2021; Bupphathong S., *et al.*, 2022).[16,17] Nazir *et al.* compounded GelMA with 6-deoxy-6-diethylamide cellulose to create a hydrogel wound dressing with improved elongation at break (61.3%), significantly enhancing the wound healing rate in rats (Nazir F., *et al.*, 2021).[18] The molecular structure of GelMA contains numerous hydroxyl groups, providing excellent hydrophilic properties. Its internal cross-linking network structure can retain a large amount of water, maintaining a moist microenvironment at the wound site and promoting tissue regeneration (Han Y., *et al.*, 2023).[19] GelMA also features rapid photocrosslinking properties, forming a network-structured gel after a brief photocrosslinking process. When functional components such as drugs and growth factors are added to the GelMA solution, they are quickly immobilized within the gel without being damaged (Dong Y., *et al.*, 2022; Cao C., *et al.*, 2021).[20,21] By adjusting parameters such as photocrosslinking time and GelMA concentration, the release efficiency of drugs can be controlled, allowing their effects to be fully utilized.

In order to further accelerate the process of repairing chronic wounds, researchers have initiated a broader range of novel dressings, including dressing materials, the addition of growth-promoting factors, and their combined use (Jiang J., *et al.*, 2023).[22] The performance of platelet-rich gel (PRG), a biomaterial that promotes wound healing and tissue regeneration, is influenced by its composition and structure (Song Y., *et al.*, 2023).[23] To date, several studies have investigated hydrogels that incorporate PRP as a component. Liu G. *et al.* developed a thermosensitive chitosan (CS) wound dressing hydrogel containing β-glycerophosphate (GP), hydroxypropylcellulose (HPC), graphene oxide (GO), and platelet-rich plasma (PRP). This hydrogel enhanced antimicrobial effects and promoted wound repair (Liu G., *et al.*, 2024; Zhang J., *et al.*, 2022).[24,25] However, the combination of antibacterial activity and photothermal properties in biomedical hydrogels containing PRP has not yet been achieved.

Metal–organic frameworks (MOFs) are porous materials composed of metal clusters or metal ions and organic ligands, characterized by high porosity and a large specific surface area. They are easily surface-functionalized, and their physicochemical properties can be flexibly tuned (Li B., *et al.*, 2012; Zhu Q. L., *et al.*, 2014).[26,27] By selecting suitable metal ions and organic ligands, MOFs can be endowed with various bioactive capabilities, making them highly promising for biological applications (Wu M. X., *et al.*, 2017; Guo Y., *et al.*, 2022; Lim J. Y. C., *et al.*, 2023).[28–30] Due to their unique porous structure and tunable composition, MOFs can serve as universal carriers for applications such as tumor therapy, disease diagnosis, and sterilization (Lelouche S. N. K., *et al.*, 2022).[31] Among these, Zn^{2+} is a common antimicrobial metal ion known for its ability to disturb bacterial microenvironments and disrupt ion channels in membranes, giving zinc-based MOFs significant potential in antimicrobial applications (Li R., *et al.*, 2021).[32] Comparative studies of zinc-based MOFs, such as ZIF-8 and MOF-5, have shown that the release rate of metal ions critically influences their antimicrobial properties. This study underscored the importance of regulating the release rate of metal ions when designing antimicrobial materials, providing a theoretical basis and guidance for developing more efficient antimicrobial MOFs (Costa B. A., *et al.*, 2023; Younis S. A., *et al.*, 2020).[33,34] However, there are fewer reports on the use of PRP gels in conjunction with the porous and highly adsorbable nature of MOFs. The effects of MOFs on the properties and potential applications of PRP gels have not been fully explored, warranting further investigation.

Based on the above analysis, the focus of this paper would be to investigate the effect of combining MOF and PRP on the structural characteristics and biological properties of GelMA dressings. The experimental schematic for this study was shown in Fig. 1. Firstly, PRP was adsorbed onto MOF and then added to GelMA to investigate the effects of these additives on the cross-linking degree, mechanical properties and biological properties

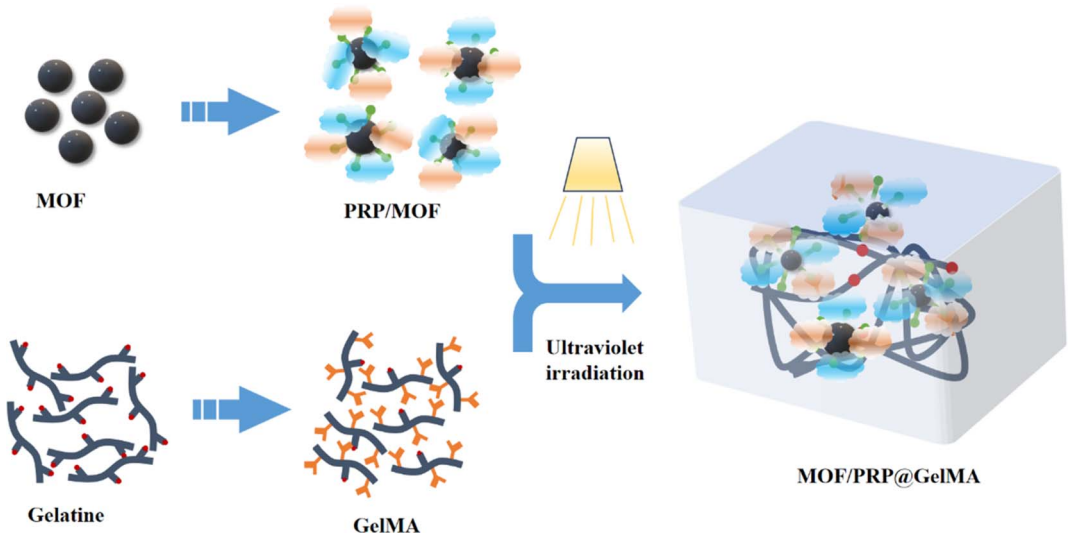

Fig. 1 Study scenario diagram.

of GelMA. Meanwhile, as a control group, MOF and PRP were added to GelMA alone, respectively. Subsequently, *in vitro* cellular experiments were conducted to evaluate the biocompatibility of the gels, and their efficiency in promoting wound healing would be explored using a rat chronic infected wound model. This study aims to provide a robust scientific basis for the development of novel biomedical materials capable of promoting tissue growth.

2. Materials and methods

2.1 Materials

2.1.1 Synthesis of gel MA. Added 10 g of gelatin to 100 mL of deionized water and solubilized at room temperature for 1 hour. Placed the gelatin solution in a constant temperature water bath at 60 °C and stirred until completely dissolved. Under light-avoiding conditions, added 6 mL of methacrylic anhydride dropwise to the gelatin solution at a rate of 1 mL min^{-1}. Continue the reaction for 3 hours at a constant temperature of 50 °C with stirring at 150 rpm. Transferred the reacted solution into 8–14 kDa dialysis bags and dialyze in deionized water at 50 °C for 7 days, changing the deionized water every 12 hours. Centrifuged the dialysate at 3000 rpm for 10 minutes, collect the supernatant, and placed it in a refrigerator at −80 °C overnight. Freeze-dry the supernatant for 3 days to obtain the GelMA.

2.1.2 PRP extraction. Collected mouse whole blood into anticoagulant tubes. Centrifuged the blood at 2500 rpm for 10 minutes at 4 °C. After centrifugation, a clear demarcation line should appear. Aspirated the supernatant and the solution 1 mm below the interface into a clean centrifuge tube. Centrifuged this solution at 3200 rpm for 8 minutes. Removed the top 3/4 of the supernatant and discarded the erythrocyte precipitate at the bottom. The remaining solution is PRP. Added dimethyl sulfoxide (DMSO) to the PRP to achieve a final concentration of 5%, mix well. Stored the prepared PRP at −80 °C for future use.

2.1.3 Preparation of MOF@GelMA. The MOFs used in the experiments were Zn-MOFs developed by the Laboratory of Inorganic Chemistry of Nanning Normal University, and their morphology was shown in Fig. 2b as a single-crystal structure in the shape of a bar.[35] Firstly, 0.5 mg of MOF powder was added to 10 mL of lithium phenyl-2,4,6-trimethylbenzoyl phosphinate (LAP, BIOMART.CN, China) at a concentration of 20 g L^{-1} and shaken well. Subsequently, 90 mL of GelMA solution at a concentration of 100 g L^{-1} was added and thoroughly mixed, ensuring the mixture was kept away from light.

2.1.4 Preparation of PRP@GelMA. Dissolve 10 g of dried GelMA in 100 mL of platelet-rich plasma solution with a 50% volume fraction. Then, add 20 mg of LAP and mix thoroughly, ensuring the solution is kept away from light.

2.1.5 Preparation of MOF/PRP@GelMA. 0.5 mg of MOF powder was added to 100 mL of PRP with a 50% volume content and stirred for 30 minutes to ensure that the porous MOF particles fully adsorbed the growth factors present in the PRP. Then, 10 g of GelMA was added and mixed thoroughly, and finally 20 mg of ALP was added and mixed away from light and set aside.

2.2 Structural analysis for gels

The freeze-dried gels were fractured, and gold was sputter-coated onto the sections for SEM analysis. The microstructure of the gels was observed using a scanning electron microscope (SEM). Additionally, the functional group structure of the gels was analyzed using infrared spectroscopy at a resolution of 4 cm^{-1}.

2.3 Zn^{2+} ion release analysis

The Zn^{2+} release test was conducted using the zincon spectrophotometric method. To monitor the Zn^{2+} released from the MOF@gelMA and PRP/MOF@gelMA constructs, 1 mg samples of each gel were immersed in 2 mL of PBS (pH 7.35) at 37 °C. Throughout the process, the leaching solution was collected at designated intervals and analyzed *via* zincon spectrophotometry at 620 nm using an enzyme-labeled instrument. The standard curve generated was then employed to determine the cumulative amount of Zn^{2+} released.

2.4 Analysis of mechanical properties for gels

To test the compression modulus, the different gels were formed into cylindrical samples with a height and diameter of 20 mm each. An electronic universal testing machine was used to measure the compression modulus of the hydrogel samples. The maximum compressive strength data were recorded until the hydrogels were completely disintegrated. The compression speed was set at 0.05 mm s^{-1}.

2.5 *In vitro* antimicrobial analysis

E. coli and *S. aureus* were used to evaluate the antimicrobial properties of the gels. The bacteria were resuscitated and their concentration was adjusted to 10^6 CFU mL^{-1}. Then, 100 μL of the bacterial solution was added to a pre-UV-sterilized gel sample. After incubating the samples in a shaker at 37 °C for 12 hours, the bacterial suspension was spread on agar culture plates and further incubated at 37 °C for 24 hours. Finally, bacterial colonies were counted, and the antimicrobial efficacy was calculated.

2.6 Biocompatibility analysis

CCK-8 kit (NCM Bio, Suzhou, China) was used to detect the proliferation ability of cells on the gel surface. After placing the gel in a 24 well plate, HUVECs were inoculated onto there surface (1.0×10^4 cells per well) and then incubated in a cell culture incubator for 1, 3 and 5 days. After absorbing and discarding the culture medium, cleaning 3 times with PBS, and adding 500 μL complete culture medium containing 10% CCK-8 solution to each well. The 24 well plate was taken back to the cell incubator for 4 h. After complete stability, 200 μL of reaction solution was pipetted and placed in a 96 well plate, then its absorbance value at a wavelength of 450 nm was detected using an enzyme labeling instrument (Biotek, USA).

Cell viability in different groups of gels were carried out by live/dead staining (Invitrogen, USA). The gels were placed in 24 well plates and co-cultured for 48 h with third-generation

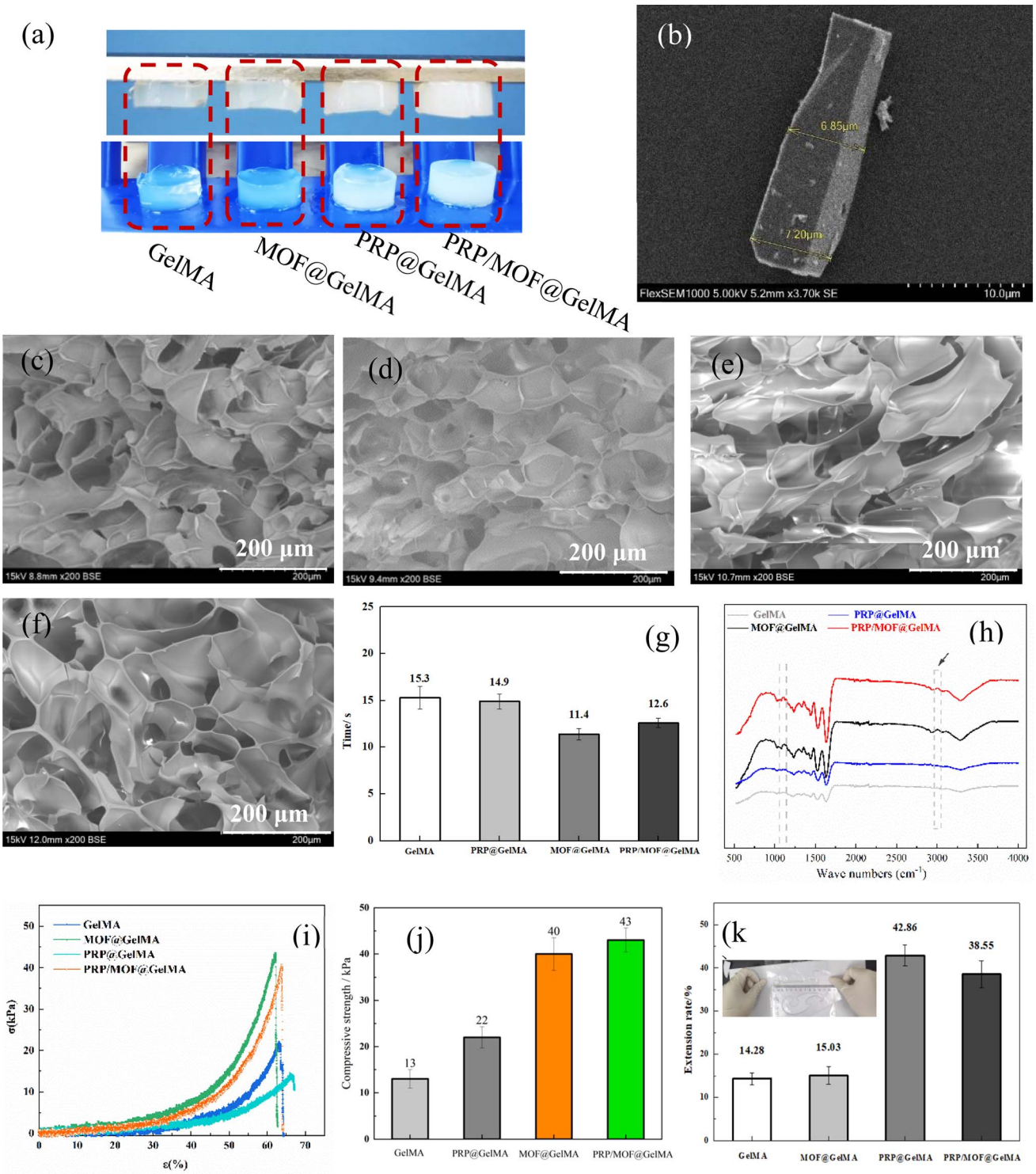

Fig. 2 Macroscopic view of the different gels (a), SEM morphology of MOF particles (b), SEM morphology of gels with different compositions ((c) GelMA, (d) MOF@GelMA, (e) PRP@GelMA, (f) PRP/MOF@PRP), crosslinking time of different gels (g), FT-IR spectra of different gels (h), compression strength analysis (i), quantitative analysis results for (i) and (j), tensile deformation (k).

HUVECs (1.0×10^4 cells per well) inoculated on their surface. After that, medium was removed, and cells were carefully stained with live/dead staining kit for 15 min away from light. Then, a fluorescence microscope (Zeiss, Germany) was used to observe the samples.

Cellular apoptosis was assessed using the Annexin V-FITC/PI apoptosis kit in conjunction with a flow cytometer (BD Bioscience, USA). HUVECs were plated in 6 well plates at a density of approximately 50 000 cells per well. After a 72 hours incubation, the cells were digested with trypsin and rinsed with PBS.

Subsequently, they were centrifuged at 1500 rpm for 5 minutes. The cell pellet was then resuspended in 500 μL binding buffer, to which 5 μL each of Annexin V-FITC and propidium iodide (PI) were added. After a 5 minutes incubation at room temperature, apoptosis was analyzed using the flow cytometer and FACSDiva software.

2.6.1 Evaluation of Angiogenesis. To observe the angiogenic capability of gels, Matrigel (Corning, USA) was applied. The working Matrigel was made by mixing theMatrigel and the extracts from different coatings at a ratio of 1 : 1. Before seeding cells, 250 μL of working Matrigel was added into each well and incubated at 37 °C for 30 min to gel. Next, HUVECs (3×10^5 cells per well) were seeded into each well in coating extracts. Following incubation at 37 °C with 5% CO_2, the plate was observed at 4 h using an optical microscope. Results were analyzed *via* Image J.

2.6.2 Cell migration assay. In 6 well plates, HUVECs at a concentration of 5×10^5 cells per well were inoculated into blank (control) and gels steed for culture. When the cells had grown all over the culture dish, the tip of a sterile pipette was used to make a scratch on the adherent cell layer, and then the cell migration was observed by microscope after 24 and 48 hours.

2.6.3 Hemolysis. Whole blood from SD rats (provided by the Animal Center of Guangxi Medical University) was used to evaluate the hemolytic properties of the gels. First, fresh blood was centrifuged at 1500 rpm for 10 minutes to obtain red blood cells (RBCs). The erythrocyte suspension was then diluted with PBS and incubated with the prepared gel (1 cm × 1 cm) for 1 hour at 37 °C. Deionized water and PBS were used as positive and negative control groups, respectively. After incubation, the samples were centrifuged at 5000 rpm for 15 minutes. The hemolysis rate was determined using a UV-Vis spectrophotometer at an absorbance of 540 nm (Abs). The formula for calculating the hemolysis rate is shown below:

$$\text{Hemolysis rate } (\%) = \frac{A_p - A_b}{A_w - A_b} \times 100\% \quad (1)$$

where A_p was Abs at 540 nm for each group of samples, A_b and A_w were Abs for saline and deionized water groups, respectively.

2.7 *In vivo* experiments in animals

To study the effect of different gels on chronic wound healing, a full-thickness skin wound model infected with *S. aureus* was created on the dorsal region of C57 mice. Specifically, male mice weighing 20–25 g were anesthetized, their dorsal hair was shaved, and a full-thickness skin wound (~6 mm in diameter) was created. Then, 10 μL of a solution of *S. aureus* (1×10^7 CFU mL^{-1}) was added dropwise to the wound to establish an infected wound model. The mice were randomly divided into five groups, with their wounds treated with saline (blank control group), GelMA, MOF@Gel, PRP@Gel, and PRP/MOF@Gel. This study was performed in strict accordance with the NIH guidelines for the care and use of laboratory animals (NIH Publication No. 85-23 Rev. 1985) and was approved by the Animal Care & Welfare Committee of Guangxi Medical University (Guangxi, China).

Table 1 Primer sequence list

Target gene	Primer sequence (5′–3′)	T_m	Location
IL-6-forward primer	GGCGGATCGGATGTTGTGAT	62.4	394–413
IL-6-reverse primer	GGACCCCAGACAATCGGTTG	62.5	592–573
VEGF-forward primer	GAGGTCAAGGCTTTTGAAGGC	61.5	139–159
VEGF-reverse primer	CTGTCCTGGTATTGAGGGTGG	61.5	298–278
PDGF-forward primer	ACTTCTGTTGCTACACGAAGC	60.6	24–44
PDGF-reverse primer	CGGTTGAGTCAGTGGAGTCC	61.9	184–165

2.7.1 Wound healing. The wounds of mice in each group were observed and analyzed for healing at 0, 1, 3, 5, 7, 9, 10, and 14 days after intervention. The wound area was calculated using ImageJ image analysis software. The formula for calculating the wound healing rate is shown below:

$$\text{Wound healing rate} = \frac{\text{Initial area of wound} - \text{Area of unhealed wound}}{\text{Initial area of wound}} \times 100\% \quad (2)$$

2.7.2 Histologic analysis of wounds. To evaluate epidermal regeneration and inflammatory response, wound skin samples were collected from different rats on days 7 and 14, respectively. These samples were fixed with 4% paraformaldehyde, paraffin-embedded, and then transversely cut into 4 μm-thick sections. The sections were subsequently stained and analyzed using hematoxylin and eosin (HE) and Masson's trichrome staining.

2.7.3 Analysis of IL-6, VEGF, and PDGF expression. Wounded skin tissues from mice on day 7 were collected, and RNA was extracted using the OMEGA Tissue RNA Extraction Kit. Reverse transcription was then performed using Thermo RevertAid™ Master Mix with DNase I-LBID (Pre-mixed Reverse Transcription Kit). PCR amplification reactions were carried out using 2x S6 Universal SYBR qPCR Mix-EnzyArtisan and an RT-PCR instrument. The relative mRNA expression levels of the target genes were calculated using the 2-ΔΔCt method, and the data were statistically analyzed. GAPDH served as the internal reference gene, while the target genes included IL-6, VEGF, and PDGF. The primer sequences used in this experiment are shown in the Table 1.

2.8 Statistical analysis

Data were statistically analyzed using Graphpad, and each experiment was performed at least three times ($n > 3$), and data were expressed as mean ± standard deviation using one-way ANOVA and least significant difference (LSD) *t*-test. *P*-Value < 0.05 is statistically significant: (*) represents $p < 0.05$, (**) represents $p < 0.01$, (***) represents $p < 0.001$.

3. Results and discussion

3.1 Preparation and characterization of gels

In this study, it was expected that the prepared dressing can be applied to skin and wet wound care, so it needed to have a good adhesion ability to adhere stably to the wound area. The effect of different additives on the structural and mechanical

properties of GelMA gel was shown in Fig. 2. Fig. 2a illustrates that the GelMA gels, modified with various additives, were capable of adhering invertedly to a flat surface and remained securely in place despite gravitational forces, thereby demonstrating their excellent adhesive properties. It could also be observed that the addition of MOF particles had minimal impact on the appearance of the GelMA. In contrast, the incorporation of PRP led to a gradual change in the color of the GelMA, causing it to take on a milky white hue. Fig. 2b displays the micromorphology of the MOF, revealing a rod-like single crystal structure. The ability of the MOF to fluoresce under UV light suggested its potential role in light energy conversion within photocrosslinked gels.[35] The SEM morphology (Fig. 2c–f) showed that the gels showed an interconnected cavity structure with uniform pores and good plasticity. With the increase of MOF particles, the pores of the gel gradually became smaller and elliptical (Fig. 2d); while the addition of PRP made the pores of the gel larger and longer (Fig. 2f). When MOF and PRP were added in mixture, the pore size of the gel was in between, reflecting a moderate modulation effect. Fig. 2g illustrates the impact of different additives on the cross-linking time of GelMA. Notably, the addition of MOF particles reduced the cross-linking time from ~15.3 s to ~11.4 s, while the effect of PRP was negligible. When PRP-modified MOF (PRP/MOF) was added, the energy conversion functionality of the MOF remained unaffected, and the cross-linking time of the GelMA was approximately 12.6 s. This suggested that MOF particles played a significant role in accelerating the GelMA cross-linking process, while the presence of PRP did not interfere with this accelerating effect.

FT-IR analysis (Fig. 2h) of the gels revealed minimal changes in the absorption peaks of the PRP-added GelMA. This may be due to the influencing factors in PRP being primarily proteins, which had a molecular weight similar to that of the gel. As a result, there was minimal change in the degree of freedom within the system and, consequently, little impacted on the polymerization degree of the gel. In contrast, the presence of MOF resulted in the appearance and enhancement of methylene absorption peaks around 2900 cm^{-1}. In MOF, Zn is typically six-coordinated, with three vacant orbitals after the removal of a water molecule. This facilitated cross-linking and increases the degree of freedom within the system.[35] During the photopolymerization process, this allowed for the provision of more active groups during the chain growth phase. MOF acted as a chain transfer receptor, forming new active species and inducing further chain growth.[36] This deepened the reaction extent and increases the polymerization degree of the hydrogel.

The mechanical properties of the gels were analyzed, as shown in Fig. 2i–k. Among them, Fig. 2i shows the compressive stress–strain curve, and it can be observed that the addition of PRP caused an increase in the compressive strain of the gel, while the addition of MOF decreased its strain. The results of the compressive stress fitting were shown in Fig. 2j, the addition of PRP reduced the compressive modulus of the gel from approximately 22 kPa to around 13 kPa, while significantly enhancing their tensile properties, allowing them to stretch up to 140% of their original length (Fig. 2k). However, the combined addition of PRP and MOF did not significantly affect the extensibility of the hydrogels but markedly improved their compressive strength, increasing it from approximately 22 kPa to over 40 kPa (Fig. 2j). This improvement could be attributed to the interaction between the abundant proteins and other bioactive substances in PRP with the GelMA hydrogel network, leading to increased porosity.[15] Meanwhile, the inclusion of MOF particles introduced additional coordination bonds that acted as extra cross-linking points, increasing the network density. This results in a modest increase in extensibility but significantly enhances the compressive strength and overall stability of the material.

3.2 Gel solubility and swelling analysis

The solubility of biomaterials is a crucial indicator for their application in biomedical fields. In this experiment, various gels were immersed in PBS (pH = 7.4) solution to test their solubility, and the results are displayed in Fig. 3. It was observed that PRP@GelMA, MOF@GelMA, and PRP/MOF@GelMA began to dissolve on the 5th day of immersion, reached about 50% dissolution by the 8th day, and completely dissolved by the 12th day. In contrast, the GelMA group had not fully dissolved by day 12 and remained intact in shape. SEM analysis revealed that the incorporation of PRP, MOF, or PRP/MOF caused the internal network structure of the gel to become looser, reducing the cross-linking strength, which facilitated the degradation of the gel. This indicated that the degradation rate of the gel could be modulated by adding PRP/MOF. The gradual degradation of the gel not only promoted the release of PRP and its growth factors, enhancing cell growth and wound healing, but also contributed to the inhibition of bacterial infection through the release of Zn^{2+}.

The swelling properties of the gel material play a crucial role in the wound healing process by enabling rapid absorption of exudate in the early stages, thereby preventing the exudate from hindering cell growth and healing. Fig. 3b illustrates the swelling performance of different gels in PBS solution. It was observed that each gel group exhibited a high swelling rate within the first 12 hours, after which the swelling rate stabilized. Notably, the addition of PRP significantly increased the swelling rate, reaching more than six times the original volume. Micro-structure analysis indicated that the inclusion of PRP increased the porosity of the gel, leading to higher internal osmotic pressure, which facilitated the absorption and retention of water molecules, thereby enhancing the gel's swelling rate. Additionally, the combined addition of MOF and PRP further increased the swelling rate of the gel, reaching up to seven times the original volume. Therefore, PRP/MOF@GelMA demonstrates excellent potential for wound healing applications.

3.3 Analysis of antimicrobial properties of gels

Efficient antimicrobial properties are essential for wound healing as it prevents the potential risk of wound infection. As shown in Fig. 4, the contact antimicrobial method was used to test the inhibitory properties of MOF and PRP additions against two species of *S. aureus* and *E. coli*. Among them, PRP/GelMA

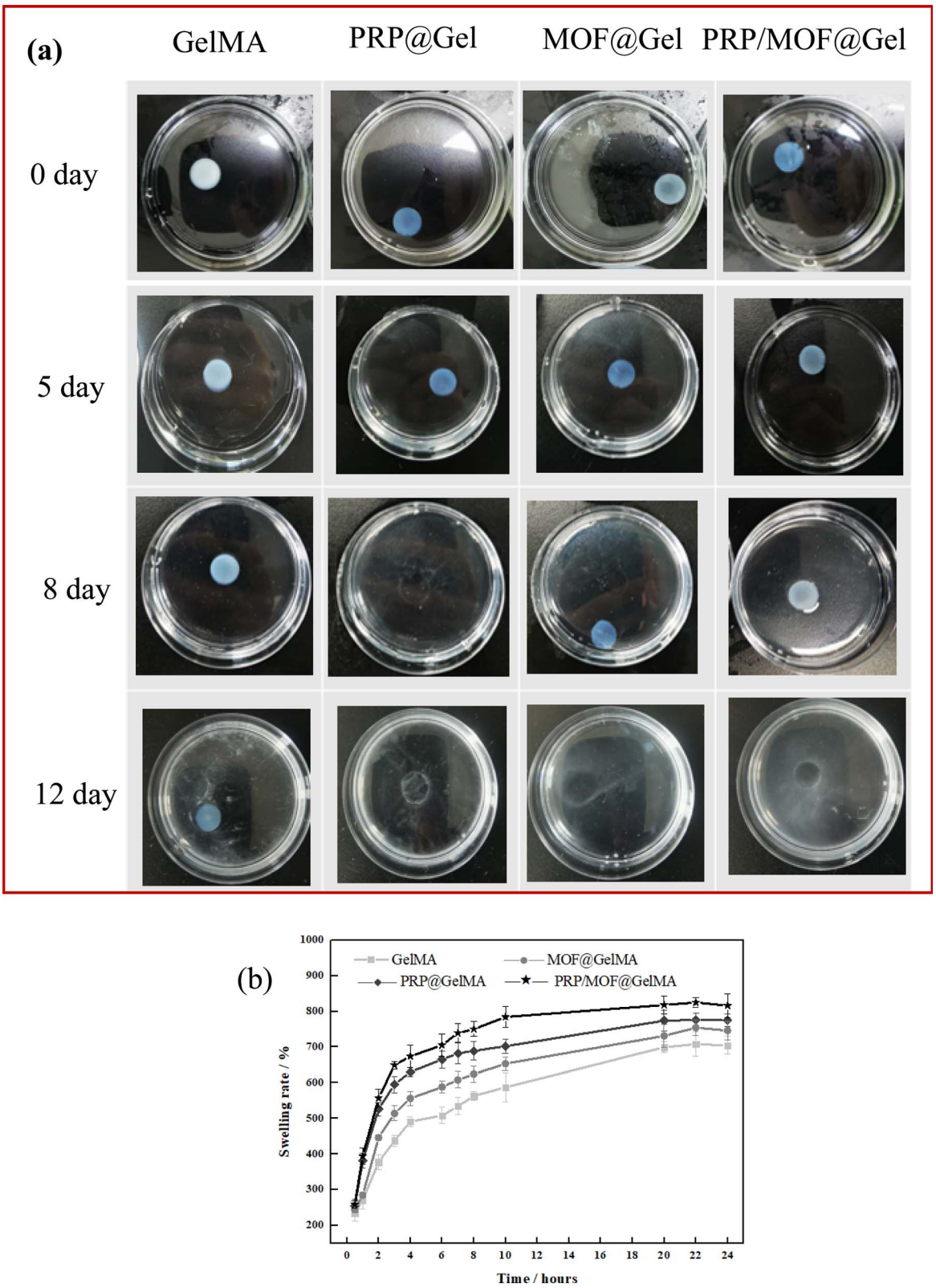

Fig. 3 Degradation (a) and the swelling rate (b) of different gels in PBS with at 37 °C, pH = 7.4.

showed lower inhibitory effects on both bacteria, with inhibition efficiencies of 76.4% and 70.1% for *S. aureus* and *E. coli*, respectively. While PRP itself may not directly have a strong bactericidal effect, when platelets were activated they release a variety of antimicrobial peptides and cytokines that inhibit bacterial growth and enhance the immune system response.[37]

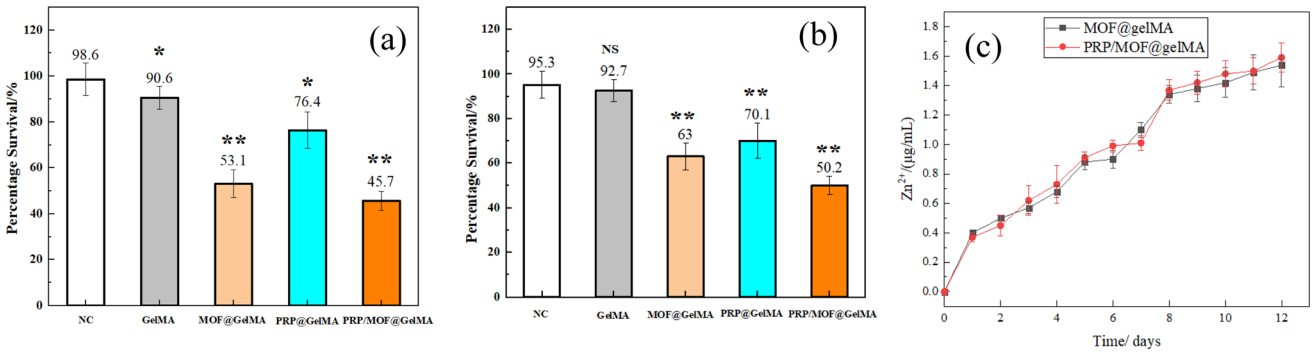

Fig. 4 Antibacterial analysis of different gels for (a) *S. aureus*, (b) *E. coli*, (c) Zn^{2+} release curve (*$P < 0.05$, **$P < 0.01$).

Among the different gels, the one with better inhibition effect was PRP/MOF@GelMA, which inhibited *S. aureus* and *E. coli* by 45.7% and 50.2%, respectively. The release of Zn^{2+} from various gels was analyzed, and it was found that, after 12 days of immersion in PBS solution, the Zn^{2+} concentrations for MOF@GelMA and PRP/MOF@GelMA were approximately 15.8 μg mL^{-1} and 16.1 μg mL^{-1}, respectively, as illustrated in Fig. 4c. This was thus attributed to the release of Zn^{2+} from the MOF particles as well as the action of growth factors in PRP, which together enhance the overall antimicrobial effect.

3.4 Bio-compatibility analysis of gels

During the wound healing process, the regeneration of skin tissue depends on cell survival and growth, making it essential for the gel to have excellent bio-compatibility. Fig. 5a–c shows live–dead staining results for different cell groups. After 24 hours of co-culture with the gel material, cells in all groups grew well, and no obvious dead cells were observed, indicating low cytotoxicity of the gel material in all groups. As shown in Fig. 5q, cells exhibited a good proliferation rate when co-cultured with different gels. On the first day, cells in the blank control group proliferated slightly faster than those in the other groups, likely because they could proliferate rapidly in an undisturbed culture medium environment. However, after 3 days, the cell proliferation rate in the gel groups surpassed that of the blank control group, with the PRP-containing groups showing particularly high proliferation rates. There was little difference in proliferation rates between the PRP/MOF@GelMA and PRP@GelMA groups. By day 5, cell proliferation in all co-culture environments approached its peak. At this point, the OD value of the PRP/MOF@GelMA group reached the highest level, indicating that PRP within the MOF particles continued to release and promote cell proliferation even after the culture medium environment became saturated. Overall, the PRP gel demonstrates a significant potentiating effect during wound repair.

On different gels, cells exhibited a polygonal structure with extensions reaching out in various directions, indicating good cell viability (Fig. 5e–h). Notably, the cell status was optimal on PRP@GelMA and PRP/MOF@GelMA, suggesting that these hydrogels release more growth factors, providing additional bioactive sites for cell growth and thereby promoting cellular proliferation. Comparative results showed that the addition of PRP increased both cell number and expansion capacity.

Wound recovery is inextricably linked to angiogenesis, so we conducted experiments on the effect of gels for angiogenesis, and the results were shown in Fig. 5i–l. Similarly, factors such as PRP and MOF inhibited cellular angiogenesis, as evidenced by impeding the formation of tubes, nodes, and branches in HUVECs (Table 2). Regardless of the existence of PRP, the angiogenic effect of the HUVECs was promote, and the best results were demonstrated in the PRP@GelMA. It was demonstrated that the inclusion of MOF did not inhibit angiogenesis, whereas the growth factors in PRP promoted the angiogenesis.

Apoptosis was tested using flow cytometry on cells under co-culture of different coatings and the results were shown in Fig. 5m–p. HUVECs co-cultured with different gels for 72 hours detected little difference in apoptosis rate between groups, but the apoptosis rate was slightly decreased by the addition of PRP or PRP/MOF. From Fig. 5r, it can be observed that the apoptosis rate in PRP@GelMA was 1.79%. This was because PRP contained a variety of growth factors that could be rapidly released during the cell culture, promoting cell proliferation. In contrast, the apoptosis rate in PRP/MOF@GelMA increased to 2.79%. This increase was attributed to the MOF particles adsorbing PRP to some extent, but not being able to release it quickly within a short period, thus failing to show its advantages in the first three days of cell growth. However, in longer cell proliferation experiments, the advantage of PRP/MOF@GelMA became apparent, as it could continuously release the growth factors required for cell growth, thereby maintaining a high growth rate (Fig. 5q).

Cell migration ability also plays a crucial role in wound healing. We investigated the effect of different gels on cell migration capacity by scratch experiments. The co-cultured HUVECs cells in both PRP and PRP/MOF groups exhibited faster migration growth compared to the control group (Fig. 6a and b). After 24 hours of co-culture, the healing rate of the scratches in the experimental group was more than 75%, while the healing rate of the scratches in the control group was less than 30%. After 48 hours, the scratches in the experimental group had completely healed, while the healing rate in the control group was still below 50%. The results showed that PRP/

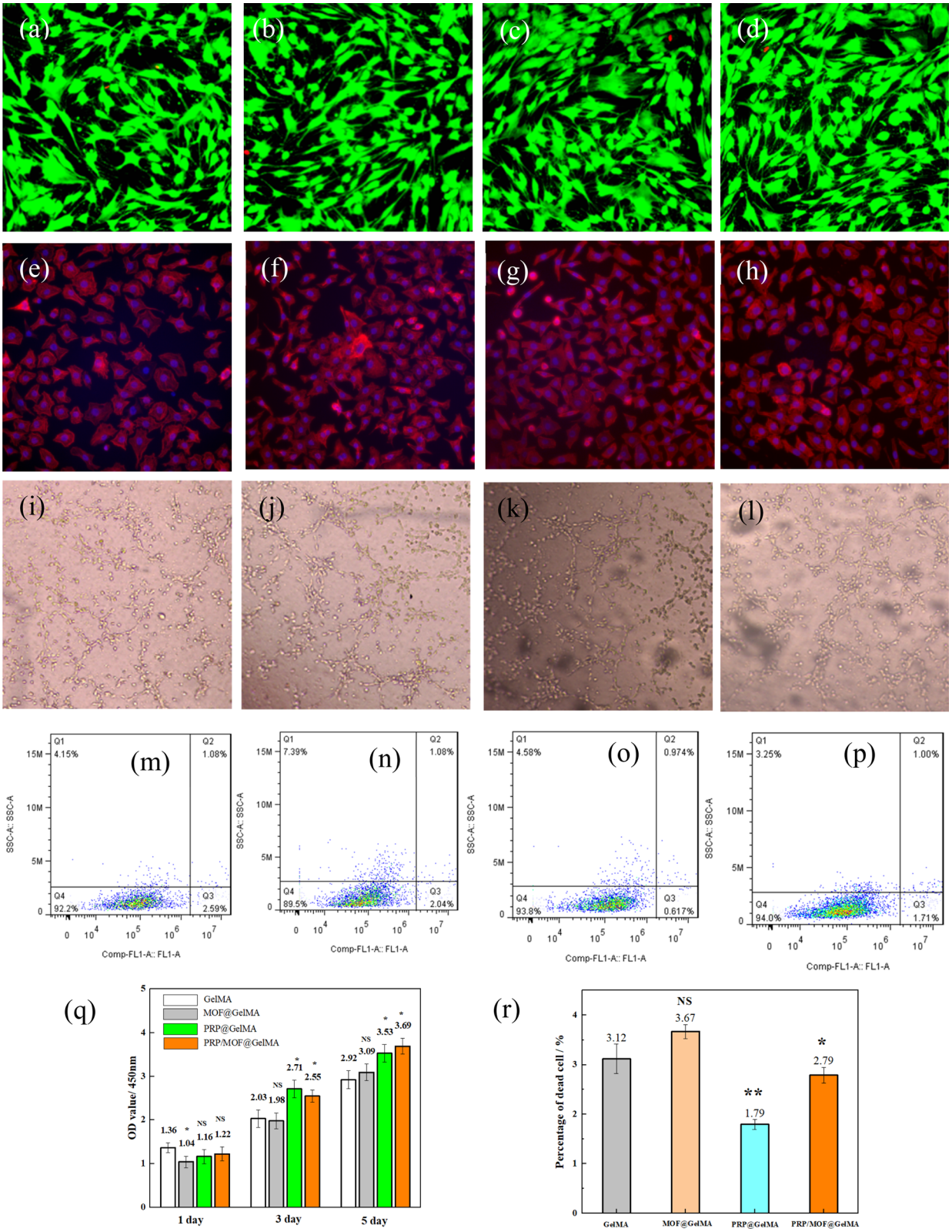

Fig. 5 Live/dead staining analysis for different cells ((a) GelMA, (b) MOF@GelMA, (c) PRP@GelMA, (d) PRP/MOF@GelMA), fluorescent staining of cells with different gels ((e) GelMA, (f) MOF@GelMA, (g) PRP@GelMA, (h) PRP/MOF@GelMA), effect of gels on cellular vascularization ((i) GelMA, (j) MOF@GelMA, (k) PRP@GelMA, (l) PRP/MOF@GelMA), apoptosis evaluation of the cells grown on the gels ((m) GelMA, (n) MOF@GelMA, (o) PRP@GelMA, (p) PRP/MOF@GelMA), cytotoxicityand proliferation analysis of different gels (q), apoptosis evaluation of the cells grown on different gels (r) (*$P < 0.05$, **$P < 0.01$).

Table 2 Effect of different gels on angiogenesis of HUVECs ($x \pm s$, $n = 3$)

Sample	Tubes	Nodes	Branches
Control	7012 ± 327	207.7 ± 37.3	128.62 ± 4.6
PRP@gelMA	11 581 ± 486	421.3 ± 80.5	141.72 ± 10.8
MOF@gelMA	7942 ± 751	188.9 ± 59.7	107.37 ± 5.3
PRP/MOF@gelMA	11 395 ± 663	338.4 ± 48.1	152.07 ± 8.7

MOF hydrogel dressing could effectively promote the migration and proliferation of HUVECs cells with the potential to promote wound healing and skin regeneration. This suggested that the adsorption of PRP by MOF can realize the continuous release of growth factors and maintain the continuous migration of cells.

Since wound dressings are in direct contact with the wound during application, they must have good blood compatibility. As shown in Fig. 6d, after the prepared gel (including the control group) was thoroughly mixed with the blood erythrocytes and left to stand for a period of time, it was found that the red color in the control group was uniformly distributed, while the erythrocytes in the gel group were all precipitated to the bottom. This indicated that the red blood cells in the control group were destroyed while most of the red blood cells in the gel group were preserved intact. The absorbance of all the supernatants at 540 nm was measured by UV-Vis spectrophotometer and it was found that the hemolysis rate of all the gels was less than 4%. This is due to the predominantly gelatin component in the gel, which did not cause strong immune rejection. In particular, the presence of platelets and growth factors promoted the growth and repair of vascular endothelial cells and facilitates the maintenance of the integrity and function of the vessel wall. This helped to reduce the occurrence of non-specific blood clotting reactions and improved blood compatibility.[38]

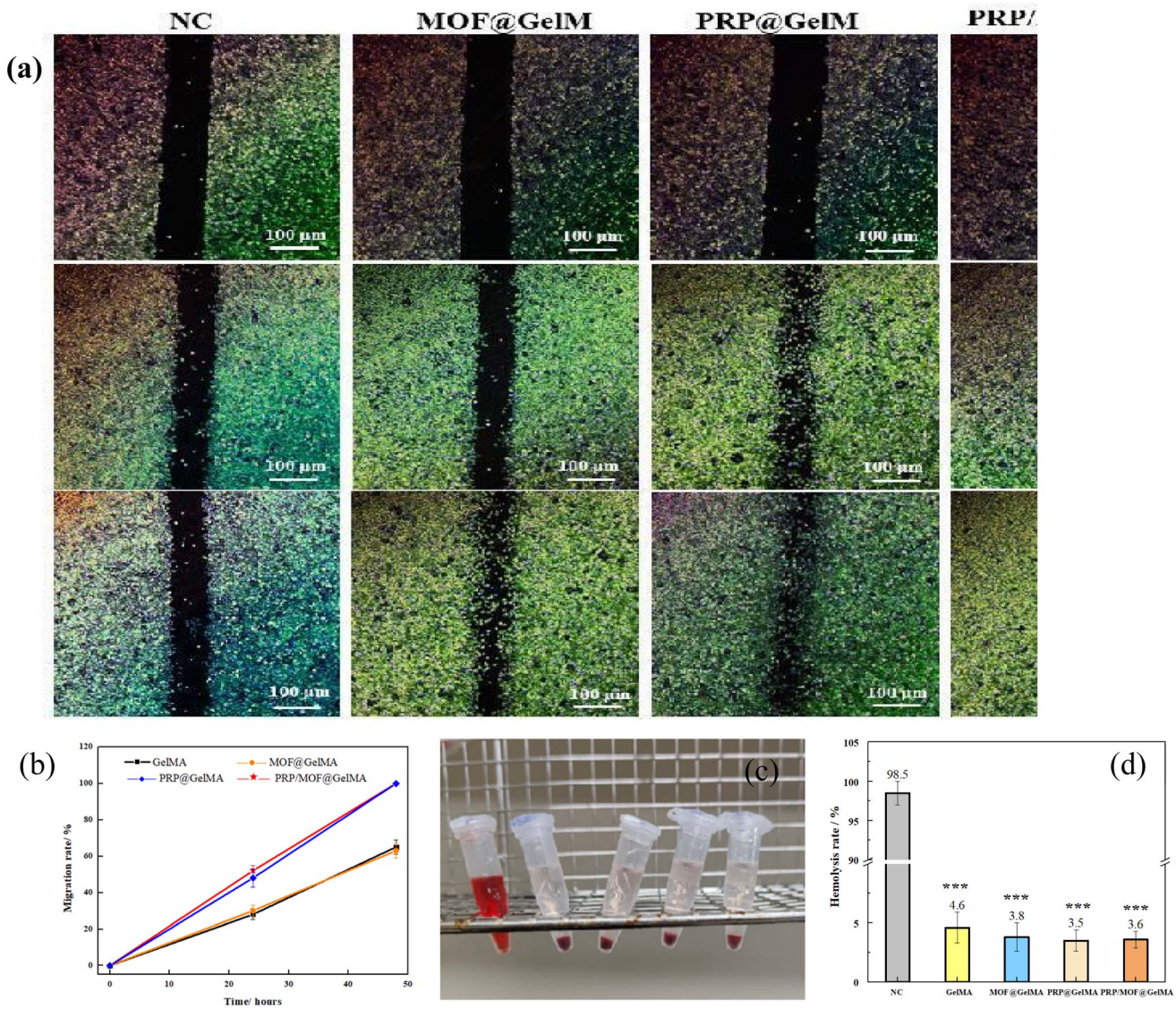

Fig. 6 *In vitro* wound healing assay of the HUVECs ((a), scale bar = 200 μm), quantitative analysis of the rate of wound closure at 48 h in the different gels (b), analysis of blood compatibility (c) and hemolysis rate of different gels (d) (***$P < 0.001$).

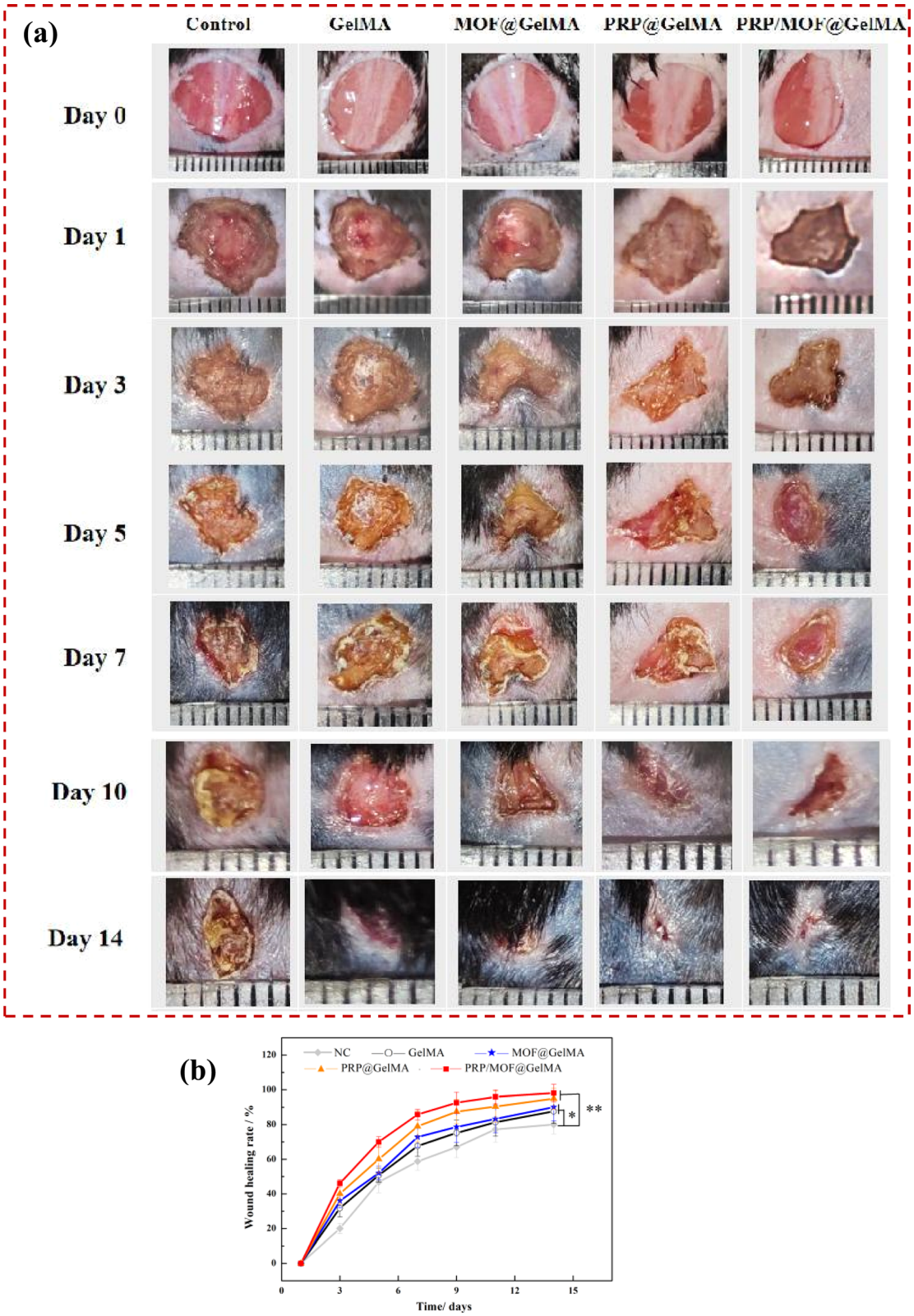

Fig. 7 (a) Wound photos of control group, GelMA, MOF@GelMA, PRP@GelMA, PRP/MOF@GelMA at 0, 1, 3, 5, 7, 10 and 14 days. (b) Wound area statistics of each group, *: compared with the control group (*P < 0.05).

3.5 *In vivo* experiments in animals

Based on the promising *in vitro* results of the gel dressing, it was anticipated to promote the healing of bacterial-infected wounds. Therefore, we evaluated the performance of this gel dressing in accelerating wound healing using a mouse bacterial infection model. The treatment groups included a blank control group, GelMA, MOF@GelMA, PRP@GelMA, and MOF/PRP@GelMA. Wound observations and tissue collections were performed on days 0, 1, 3, 5, 7, 10, and 14 to record and assess the healing of the mice wounds in each experimental group, as shown in Fig. 7a. Wound images showed that animals in the gel groups experienced an overall faster rate of wound healing. Starting from the third day, the wound area in the PRP/MOF@GelMA group was significantly smaller than in the other groups. By the 14th day, the infected wounds in the PRP/MOF@GelMA group were almost completely healed, with a wound closure rate of 98.2% (Fig. 7b). In contrast, the control group still had a larger wound closure rate of 79.3%, while the GelMA and MOF@GelMA groups had smaller wound areas of 81.5% and 82.2%, respectively. As the gel degraded, Zn^{2+} in PRP/MOF@GelMA was gradually released, effectively killing bacteria and preventing the formation of bacterial biofilm, thus reducing the inflammatory response of the wound. Meanwhile, the growth factors in PRP were continuously released, further promoting cell proliferation and tissue repair, thereby accelerating the wound healing process.

To further investigate the effect of the gel dressings on wound healing, histological analysis was performed on mouse wounds at days 7 and 14, as shown in Fig. 8. HE staining revealed inflammation in all groups, however, the PRP/MOF@GelMA and PRP@GelMA groups exhibited significantly less inflammation. The PRP/MOF@GelMA group showed the lowest level of wound inflammation, likely due to the excellent antibacterial properties of Zn^{2+} in the gel, which prevented bacterial infection and reduced inflammation at the wound site. Additionally, the growth factors in PRP promoted cell and tissue growth, further decreasing inflammation. By day 14, the PRP/MOF@GelMA group demonstrated the highest healing rate, with fewer inflammatory cells, increased fibroblasts, and clear signs of re-epithelialization and regenerated tissue structure. The wound was fully covered with epithelial cells, and the granulation tissue gap was significantly reduced. In contrast, other groups showed delayed wound healing, with incomplete wound closure, dermal defects, and incomplete epidermis. Masson staining was used to observe collagen deposition during wound healing, as shown in Fig. 8a and b. Collagen deposition gradually increased in the skin tissues of all groups, but the PRP/MOF@GelMA group exhibited the best collagen deposition with more orderly and structured collagen fibers.

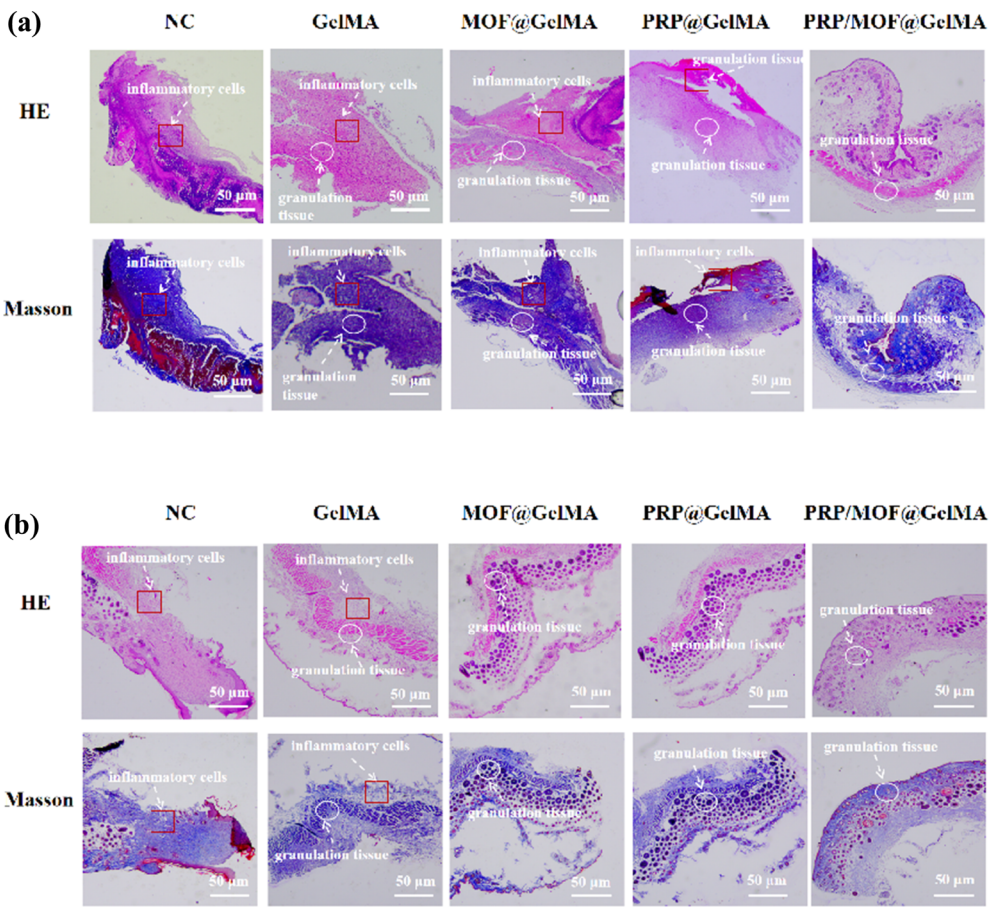

Fig. 8 HE and Masson staining of regenerative skin tissues on 7 days (a), HE and Masson staining of regenerative skin tissues on 14 days (a) and (b).

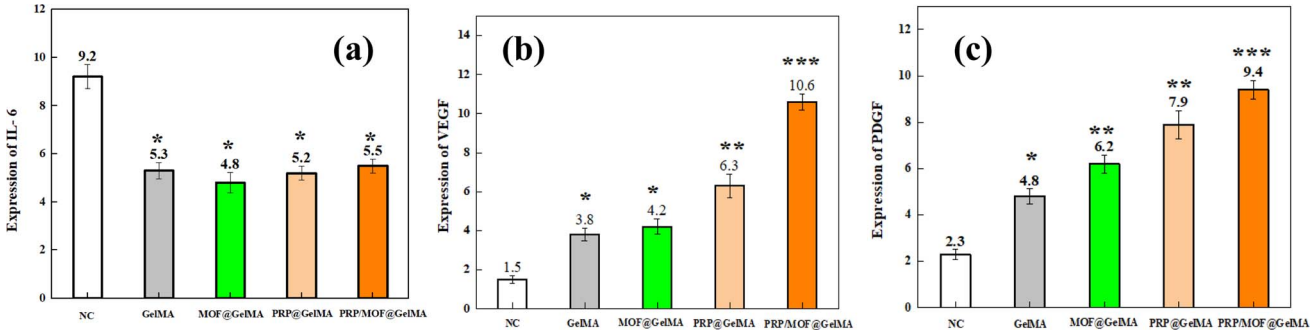

Fig. 9 Relative expression analysis of IL-6 mRNA (a), VEGF mRNA (b), and PDGF mRNA (c) in the 7th day of wound recovery (*$P < 0.05$, **$P < 0.01$, ***$P < 0.001$).

These results indicate that the PRP/MOF@GelMA gel dressing is the most effective for repairing infected wounds.

In the early stages of infectious inflammation, different pathogens stimulate monocytes and macrophages to produce IL-6 *via* Toll-Like Receptors (TLR) associated with pathogen-associated molecular patterns (PAMPs), playing a crucial role in host defense and promoting tissue growth.[39] In this experiment, the blank group showed higher IL-6 expression, while the gel groups showed slightly lower levels, though the differences among the four groups were not significant (Fig. 9a). The results confirm that vascular endothelial growth factor (VEGF) promotes capillary formation and accelerates neovascular proliferation, while platelet-derived growth factor (PDGF) promotes granulation tissue formation and fibroblast proliferation, accelerating wound healing.[40,41] As observed in Fig. 9b and c, the expression of VEGF and PDGF was highest in the PRP/MOF@GelMA group. This is likely due to the gradual release of PRP from the gel, which supports tissue cell growth.

4. Conclusion

In this study, a GelMA-based antimicrobial gel was constructed by incorporating MOF and PRP, and its therapeutic efficacy in chronic infected wounds was verified. These gels exhibited excellent adhesion and biocompatibility, significantly promoting cell proliferation, migration, and angiogenesis. Mechanistic analysis revealed that the cross-linking reaction of GelMA was disrupted by the ligand bonds of MOF and the unique protein disulfide bonds in PRP. This interference increased the internal pores of the gels, resulting in greater elongation and enhanced solubility, thereby improving their exudate adsorption efficiency in the early stages of wound healing. Experiments on bacterial infected wound models demonstrated that the MOF particles in PRP/MOF@GelMA conferred significant antimicrobial properties to the gel. Combined with the abundant growth factors in PRP, this reduced tissue inflammatory response and facilitated wound healing, providing a novel approach for the treatment of chronically infected wounds.

Data availability

The data that support the findings of this study are available from the corresponding author upon reasonable request.

Conflicts of interest

The authors declare that they have no conflict of interest.

Acknowledgements

This work was supported by the National Natural Science Foundation of China (52461043, 32360245), the Guangxi Science and Technology Major Program (No. AA24999003), Open Project of Guangxi Key Laboratory of Regenerative Medicine (202004), Middle-aged and Young Teachers' Basic Ability Promotion Project of Guangxi (2021KY0120), which are gratefully acknowledged.

References

1 H. Sorg, D. J. Tilkorn, S. Hager, J. Hauser and U. Mirastschijski, Skin Wound Healing: An Update on the Current Knowledge and Concepts, *Eur. Surg. Res.*, 2017, **58**(1–2), 81–94, DOI: 10.1159/000454919.
2 L. Qi, C. Zhang, B. Wang, J. Yin and S. Yan, Progress in Hydrogels for Skin Wound Repair, *Macromol. Biosci.*, 2022, **22**(7), e2100475, DOI: 10.1002/mabi.202100475.
3 Y. Cheng, Y. Chang, Y. Feng, *et al.*, Hierarchical Acceleration of Wound Healing through Intelligent Nanosystem to Promote Multiple Stages, *ACS Appl. Mater. Interfaces*, 2019, **11**(37), 33725–33733, DOI: 10.1021/acsami.9b13267.
4 I. Negut, V. Grumezescu and A. M. Grumezescu, Treatment Strategies for Infected Wounds, *Molecules*, 2018, **23**(9), 2392, DOI: 10.3390/molecules23092392.
5 H. S. Kim, X. Sun, J. H. Lee, H. W. Kim, X. Fu and K. W. Leong, Advanced drug delivery systems and artificial skin grafts for skin wound healing, *Adv. Drug Delivery Rev.*, 2019, **146**, 209–239, DOI: 10.1016/j.addr.2018.12.014.
6 G. C. Gurtner, S. Werner, Y. Barrandon and M. T. Longaker, Wound repair and regeneration, *Nature*, 2008, **453**(7193), 314–321, DOI: 10.1038/nature07039.
7 S. Bowers and E. Franco, Chronic Wounds: Evaluation and Management, *Am. Fam. Physician*, 2020, **101**(3), 159–166.
8 M. Volmer-Thole and R. Lobmann, Neuropathy and Diabetic Foot Syndrome, *Int. J. Mol. Sci.*, 2016, **17**(6), 917, DOI: 10.3390/ijms17060917.

9 J. Davies and D. Davies, Origins and evolution of antibiotic resistance, *Microbiol. Mol. Biol. Rev.*, 2010, **74**(3), 417–433, DOI: **10.1128/MMBR.00016-10**.

10 R. Urban-Chmiel, A. Marek, D. Stępień-Pyśniak, *et al.*, Antibiotic Resistance in Bacteria-A Review, *Antibiotics*, 2022, **11**(8), 1079, DOI: **10.3390/antibiotics11081079**.

11 K. Yue, G. Trujillo-de Santiago, M. M. Alvarez, A. Tamayol, N. Annabi and A. Khademhosseini, Synthesis, properties, and biomedical applications of gelatin methacryloyl (GelMA) hydrogels, *Biomaterials*, 2015, **73**, 254–271, DOI: **10.1016/j.biomaterials.2015.08.045**.

12 A. G. Kurian, R. K. Singh, K. D. Patel, J. H. Lee and H. W. Kim, Multifunctional GelMA platforms with nanomaterials for advanced tissue therapeutics, *Bioact. Mater.*, 2021, **8**, 267–295, DOI: **10.1016/j.bioactmat.2021.06.027**.

13 Y. Liu, T. Li, M. Sun, *et al.*, ZIF-8 modified multifunctional injectable photopolymerizable GelMA hydrogel for the treatment of periodontitis, *Acta Biomater.*, 2022, **146**, 37–48, DOI: **10.1016/j.actbio.2022.03.046**.

14 Z. Zhou, T. Deng, M. Tao, *et al.*, Snail-inspired AFG/GelMA hydrogel accelerates diabetic wound healing via inflammatory cytokines suppression and macrophage polarization, *Biomaterials*, 2023, **299**, 122141, DOI: **10.1016/j.biomaterials.2023.122141**.

15 G. Jiang, S. Li, K. Yu, *et al.*, A 3D-printed PRP-GelMA hydrogel promotes osteochondral regeneration through M2 macrophage polarization in a rabbit model, *Acta Biomater.*, 2021, **128**, 150–162, DOI: **10.1016/j.actbio.2021.04.010**.

16 K. Nuutila, M. Samandari, Y. Endo, *et al.*, In vivo printing of growth factor-eluting adhesive scaffolds improves wound healing, *Bioact. Mater.*, 2021, **8**, 296–308, DOI: **10.1016/j.bioactmat.2021.06.030**.

17 S. Bupphathong, C. Quiroz, W. Huang, P. F. Chung, H. Y. Tao and C. H. Lin, Gelatin Methacrylate Hydrogel for Tissue Engineering Applications-A Review on Material Modifications, *Pharmaceuticals*, 2022, **15**(2), 171, DOI: **10.3390/ph15020171**.

18 F. Nazir, I. Ashraf, M. Iqbal, T. Ahmad and S. Anjum, 6-deoxy-aminocellulose derivatives embedded soft gelatin methacryloyl (GelMA) hydrogels for improved wound healing applications: In vitro and in vivo studies, *Int. J. Biol. Macromol.*, 2021, **185**, 419–433, DOI: **10.1016/j.ijbiomac.2021.06.112**.

19 Y. Han, R. Dal-Fabbro, A. H. Mahmoud, *et al.*, GelMA/TCP nanocomposite scaffold for vital pulp therapy, *Acta Biomater.*, 2024, **173**, 495–508, DOI: **10.1016/j.actbio.2023.11.005**.

20 Y. Dong, M. Zhang, D. Han, *et al.*, A high-performance GelMA-GelMA homogeneous double-network hydrogel assisted by 3D printing, *J. Mater. Chem. B*, 2022, **10**(20), 3906–3915, DOI: **10.1039/d2tb00330a**.

21 C. Cao, N. Yang, Y. Zhao, D. Yang, Y. Hu, D. Yang and X. Dong, Biodegradable hydrogel with thermo-response and hemostatic effect for photothermal enhanced anti-infective therapy, *Nano Today*, 2021, **39**, 101165, DOI: **10.1016/j.nantod.2021.101165**.

22 J. Jiang, X. Li, H. Li, *et al.*, Recent progress in nanozymes for the treatment of diabetic wounds, *J. Mater. Chem. B*, 2023, **11**(29), 6746–6761, DOI: **10.1039/d3tb00803g**.

23 Y. Song, P. Li, Y. Xu, Z. Lin, Z. Deng and C. Chen, Menstrual Blood-Derived Mesenchymal Stem Cells Encapsulated in Autologous Platelet-Rich Gel Facilitate Rotator Cuff Healing in a Rabbit Model of Chronic Tears, *Am. J. Sports Med.*, 2023, **51**(7), 1872–1885, DOI: **10.1177/03635465231168104**.

24 G. Liu, Y. Yang, Y. Liu, *et al.*, Injectable and Thermosensitive Hydrogel with Platelet-Rich Plasma for Enhanced Biotherapy of Skin Wound Healing, *Adv. Healthcare Mater.*, 2024, **13**(12), e2303930, DOI: **10.1002/adhm.202303930**.

25 J. Zhang, Q. Luo, Q. Hu, *et al.*, An injectable bioactive dressing based on platelet-rich plasma and nanoclay: Sustained release of deferoxamine to accelerate chronic wound healing, *Acta Pharm. Sin. B*, 2023, **13**(10), 4318–4336, DOI: **10.1016/j.apsb.2022.11.006**.

26 B. Li, Y. Zhang, D. Ma, *et al.*, A strategy toward constructing a bifunctionalized MOF catalyst: post-synthetic modification of MOFs on organic ligands and coordinatively unsaturated metal sites, *Chem. Commun.*, 2012, **48**(49), 6151–6153, DOI: **10.1039/c2cc32384b**.

27 Q. L. Zhu and Q. Xu, Metal-organic framework composites, *Chem. Soc. Rev.*, 2014, **43**(16), 5468–5512, DOI: **10.1039/c3cs60472a**.

28 M. X. Wu and Y. W. Yang, Metal-Organic Framework (MOF)-Based Drug/Cargo Delivery and Cancer Therapy, *Adv. Mater.*, 2017, **29**(23), 1606134, DOI: **10.1002/adma.201606134**.

29 Y. Guo, Y. Li, S. Zhou, Q. Ye, X. Zan and Y. He, Metal-Organic Framework-Based Composites for Protein Delivery and Therapeutics, *ACS Biomater. Sci. Eng.*, 2022, **8**(10), 4028–4038, DOI: **10.1021/acsbiomaterials.0c01600**.

30 J. Y. C. Lim, L. Goh, K. I. Otake, S. S. Goh, X. J. Loh and S. Kitagawa, Biomedically-relevant metal organic framework-hydrogel composites, *Biomater. Sci.*, 2023, **11**(8), 2661–2677, DOI: **10.1039/d2bm01906j**.

31 S. N. K. Lelouche, C. Biglione and P. Horcajada, Advances in plasmonic-based MOF composites, their bio-applications, and perspectives in this field, *Expert Opin. Drug Delivery*, 2022, **19**(11), 1417–1434, DOI: **10.1080/17425247.2022.2130245**.

32 R. Li, T. Chen and X. Pan, Metal-Organic-Framework-Based Materials for Antimicrobial Applications, *ACS Nano*, 2021, **15**(3), 3808–3848, DOI: **10.1021/acsnano.0c09617**.

33 B. A. Costa, M. P. Abuçafy, T. W. L. Barbosa, *et al.*, ZnO@ZIF-8 Nanoparticles as Nanocarrier of Ciprofloxacin for Antimicrobial Activity, *Pharmaceutics*, 2023, **15**(1), 259, DOI: **10.3390/pharmaceutics15010259**.

34 S. A. Younis, P. Serp and H. N. Nassar, Photocatalytic and biocidal activities of $ZnTiO_2$ oxynitride heterojunction with MOF-5 and g-C3N4: A case study for textile wastewater treatment under direct sunlight, *J. Hazard. Mater.*, 2021, **410**, 124562, DOI: **10.1016/j.jhazmat.2020.124562**.

35 J. Pang, Q. Gao, L. Yin and S. Zhang, Synthesis and catalytic performance of banana cellulose nanofibres grafted with poly(ε-caprolactone) in a novel two-dimensional zinc(II)

metal-organic framework, *Int. J. Biol. Macromol.*, 2023, **224**, 568–577, DOI: **10.1016/j.ijbiomac.2022.10.145**.

36 S. Yao, J. Chi, Y. Wang, Y. Zhao, Y. Luo and Y. Wang, Zn-MOF Encapsulated Antibacterial and Degradable Microneedles Array for Promoting Wound Healing, *Adv. Healthcare Mater.*, 2021, **10**(12), e2100056, DOI: **10.1002/adhm.202100056**.

37 M. E. Nagy, K. M. Elsherbeny, A. Elshahat and H. S. Setta, Comparison between platelet-rich plasma (PRP) and mechanically emulsified fat grafts in management of chronic wounds, *Asian J. Surg.*, 2023, **46**(9), 3627–3633, DOI: **10.1016/j.asjsur.2023.01.097**.

38 N. Kalangadan, A. S. Mary, K. Mani, B. Nath, J. Kondapalli, S. Soni and V. Srinivasa Raghavan, Repurposing ivermectin and ciprofloxacin in nanofibers for enhanced wound healing and infection control against MDR wound pathogens, *J. Drug Delivery Sci. Technol.*, 2023, **90**, 105166.

39 T. Tanaka, M. Narazaki and T. Kishimoto, IL-6 in inflammation, immunity, and disease, *Cold Spring Harbor Perspect. Biol.*, 2014, **6**(10), a016295, DOI: **10.1101/cshperspect.a016295**.

40 R. S. Apte, D. S. Chen and N. Ferrara, VEGF in Signaling and Disease: Beyond Discovery and Development, *Cell*, 2019, **176**(6), 1248–1264, DOI: **10.1016/j.cell.2019.01.021**.

41 J. Zhang, W. Li, Z. Xiong, *et al.*, PDGF-D-induced immunoproteasome activation and cell-cell interactions, *Comput. Struct. Biotechnol. J.*, 2023, **21**, 2405–2418, DOI: **10.1016/j.csbj.2023.03.047**.